Elsevier Editorial System(tm) for Cold Regions Science and Technology
Manuscript Draft

Manuscript Number: CRST-D-14-00099R2

Title: A phenomenological explanation of the pressure-area relationship for the indentation of ice: Two size-effects in spherical indentation experiments

Article Type: Research Paper

Keywords: freshwater ice; pressure; indentation; size effect; strain-softening

Corresponding Author: Dr. Ekaterina Kim,

Corresponding Author's Institution:

First Author: Ekaterina Kim

Order of Authors: Ekaterina Kim; Ekaterina Kim; Erland M Schulson

Abstract: Indentation tests provide a simple means to study the inelastic behavior of ice and other materials when loaded under a compressive stress state. Such tests provide force-time plots which are often converted to pressure-area (PA) curves. For ice, PA curves are widely used in the design of ships and offshore structures. Despite their usage, and despite many attempts to relate empirical results to theory, the mechanics underlying PA curves is not clearly understood. In this paper, it is shown that by taking into account the strain-softening behavior of ice when rapidly deformed beyond terminal failure within the regime of brittle behavior, two effects can be explained: the decrease in pressure with increasing area, termed the indentation size effect; and, for a given area, the increase in pressure with increasing radius of indenter, termed the indenter radius effect. The analysis is supported using published data on freshwater, polycrystalline ice that have been obtained using spherically shaped indenters. The indentation size effect for ice reflects a similar effect found in ceramics and rock, but is opposite to the effect found in metals where, owing to strain hardening, indentation pressure or hardness increases with increasing area.

A phenomenological explanation of the pressure-area relationship for the indentation of ice: Two size-effects in spherical indentation experiments

Ekaterina Kim[*, a, b] & Erland M. Schulson [c]

[a]*Centre for Autonomous Marine Operations and Systems (AMOS), Norwegian University of Science and Technology, 7491 Trondheim, Norway*

[b]*Centre for Sustainable Arctic Marine and Coastal Technology (SAMCoT), Norwegian University of Science and Technology, 7491 Trondheim, Norway*

[c]*Thayer School of Engineering, Dartmouth College, Hanover, NH 03755, USA,*

Abstract

Indentation tests provide a simple means to study the inelastic behavior of ice and other materials when loaded under a compressive stress state. Such tests provide force-time plots which are often converted to pressure-area (PA) curves. For ice, PA curves are widely used in the design of ships and offshore structures. Despite their usage, and despite many attempts to relate empirical results to theory, the mechanics underlying PA curves is not clearly understood. In this paper, it is shown that by taking into account the strain-softening behavior of ice when rapidly deformed beyond terminal failure within the regime of brittle behavior, two effects can be explained: the decrease in pressure with increasing area, termed the *indentation size effect*; and, for a given area, the increase in pressure with increasing radius of indenter, termed the *indenter radius effect*. The analysis is supported using published data on freshwater, polycrystalline ice that have been obtained using spherically shaped indenters. The indentation size effect for ice reflects a similar effect found in ceramics and rock, but is

[*]Corresponding author. Tel.: +47 735 95710. E-mail addresses: ekaterina.kim@ntnu.no (E. Kim), erland.m.schulson@dartmouth.edu (E.M. Schulson)

opposite to the effect found in metals where, owing to strain hardening, indentation pressure or hardness increases with increasing area.

Keywords: freshwater ice, pressure, indentation, size effect, strain-softening

1. Introduction

The present study follows from Sanderson's work and is motivated by a number of observations and a number of engineering experiences at different scales on the indentation of ice. Ever since Sanderson (1988) found that the pressure to indent ice decreases with increasing area, many attempts have been made to explain the relationship. Although initially controversial, the trend of decreasing global pressure with increasing contact area now appears to have been accepted by the international engineering community (see Table 1). Upon reviewing design practices and recommendations for offshore structures and for ships, we find that it is commonly accepted that, provided ice is indented rapidly enough to impart brittle behavior, ice pressure is in accordance with Sanderson's pressure-area relationship:

$$p=CA^{q}, \qquad \textbf{[1]}$$

where C is a proportionally constant (to be discussed further), p is defined as the design (maximum/failure) load divided by either the apparent projected contact area or the local design area, and where $-0.7 \leq q \leq 0.0$. The value q=0.0 implies no size effect, which is the case for ductile behavior.

Generally, the derivation of design pressures is based on experimental data that are obtained from a variety of sources, including structure-ice interactions, ship ramming trials, borehole-jack tests, indentation tests and flat-jack tests. Also, the data come from different ice types and geometries and from different geometries of the structure. The data, therefore, are scattered, by as much as an order of magnitude or more for a given contact area. In an attempt to isolate key parameters, including confinement, contact aspect ratio, interaction rate and ice characteristics (temperature, salinity, density, grain structure, loading direction, failure mode), Timco and Sudom (2013) noted that the information is too limited to allow definitive conclusions. The challenge of understanding ice indentation and pressure-area relationships thus remains.

Several explanations of the pressure-area relationship (Eq. 1) have been offered. Some workers have attempted to explain the pressure-area relationship in terms of the flaw statistics of the specimen (Sanderson, 1988). Palmer and Sanderson (1991) used the concept of fractals combined with linear elastic fracture mechanics to explain the pressure-area effect. Palmer and Sanderson (1991) and Palmer et al. (2009) indicated that a simple dimensional argument could explain the pressure-area curve. Schulson and Duval (2009) showed that the pressure-area effect follows from Griffith's theory of brittle fracture and also from the concept of ductile-to-brittle transition. Owing to a non-uniform distribution of the force between ice and a structure (i.e., evidence of force concentration in high pressure zones (hpz's)), Palmer et al. (2009) made a distinction between the area over which a force is measured and the area that controls the force. Their explanation is based on the idea that only one hpz is present within the contact area over which the total force is measured.

1.1 Questions and approach

Noteworthy, by its absence in any of the PA explanations, is a reference to the stress-strain constitutive relationship of ice as a material. Absent, too, is the geometry of the indenter. To us, that seems like a shortcoming. Thus, this paper addresses two questions:

- Given that pressure (p) and contact area (A) are the measurable quantities and that C and q are the proportionality coefficient and exponent uniting these measurable quantities, such that $p=CA^q$, do C and q relate to the material properties of ice and to the system parameters of the indenter?
- And, for a given shape of indenter, do C and q vary with indenter size?

To those ends, our approach is first to review relevant experimental observations on the indentation of ice, and then to offer a new constitutive-based, phenomenological explanation of the effects on pressure of both indentation size and indenter radius. In the interests of clarity, we limit our discussion to the rapid indentation of freshwater, polycrystalline ice at temperatures of around –10°C by spherically shaped indenters with radii from 5 mm to 2300 mm. The term 'rapid indentation' is used here to indicate that ice exhibited characteristics of brittle compressive failure: radial cracks, saw-tooth load behavior, etc. We consider only results from tests where possible effects of sample boundaries were minimized by careful selection of the sample size, of the indenter size and of the experimental setup. In other words, we consider results only from tests that correspond to so-called full confinement indentation (as defined by Blanchet and DeFranco, 2001) or to indentation into an ice wall (Sodhi, 2001). Finally, in the interests of placing the behavior of ice within the context of materials behavior as a whole, we note that ceramics and rock also exhibit a reduction in indentation pressure with increasing area, and that metals, owing to their ability to strain harden, exhibit an inverse relationship.

To some extent our work is motivated by the findings of Masterson et al. (1992) who wrote: "*The curves [referring to PA curves] indicate that indenter curvature affects the pressures measured. In fact, Figure 16 suggests that, as plate curvature increases for a* *specific contact area, the pressure is decreasing. This may be explained by noting that a flat surface (i.e. curvature tending to zero) presents a greater degree of confinement when compared to more rounded surfaces (i.e. increasing curvature) for the same contact area*." Where we differ, is to focus not on confinement as the principal factor underlying PA relationships, although confinement is certainly present and probably a contributing factor, but to focus on ice as a material.

1.2 List of symbols

A	contact area
a	chordal radius of indentation
C, q	proportionality constants
E^*	effective elastic modulus
F	indentation force
H	hardness
k_a	Auerbach constant
p	contact pressure
p_G	global contact pressure
p_L	local contact pressure
R	indenter radius
s, f_1, f_2	numerical factors
u	penetration depth
α, β, b, c, k, k_m, m, n	material constants
ε, $\dot{\varepsilon}$	strain and strain rate, respectively
σ	representative failure stress

2. Observations

A short summary of the selected tests is given in appendix. Detailed descriptions can be found in the corresponding literature.

Figure 1 shows a summary PA plot on semi logarithmic scale, derived from the collection of indentation and impact tests (Appendix A). Data for 5 and for 12.7-mm indenters are from the constant velocity experiments by Kim et al. (2012), for 100-mm indenters are from a drop test in Timco and Frederking (1993), for 200–1280 mm and for 2300-mm indenters are from Masterson et al. (1992) and from Masterson and Frederking (1993), respectively. In using these experimental data, we assumed that the sampling frequency was high enough to capture pressure peaks.

Looking at the data in Figure 1b, one of the possible interpretations is the following: for the range of 0.003–10 m^2, there a weak PA effect. The data is highly scattered. The pressure values vary nearly by an order of magnitude for any given area. Similar thinking can be applied to the data in Figure 1a. In this case, there is really no PA effect for the contact areas between 10^{-5} and 10^{-3} m^2. However, if one looks at individual data sets (Figures 1a and 1b), two points are noteworthy: firstly, the variation of pressure with contact area exhibits self-similarity; that is, for different radii of indenter, pressure decreases with increasing (projected) contact area. And secondly, as first suggested by Masterson et al. (1992), for a given contact area the pressure is higher for larger radius indenters. Masterson's observation was made under conditions where temperature, ductile/brittle behavior and ice type were roughly the same.

As an illustration of the latter point, Figure 1b shows that if one follows up any line of constant area (e.g., A=1.0 m^2), the higher pressure values are generally seen with larger radius indenters. This point is reminiscent of an observation by Timco and Sudom (2013) who examined pressure-area data, Figure 2, for both narrow and wide structures subjected to ice action in the field. For global ice action, they observed similar pressure-area dependency, i.e., in the relationship $p=CA^q$, they found (for p in MPa and A in m^2) the exponent $q= -0.27$ and $q= -0.42$, for narrow and wide structures, respectively, while C=1.06 for narrow structures and C=6.02 for wide ones (Figure 2a). The local pressures measured on the narrow structure were lower than those measured on the wide structure (Figure 2b). Timco and Sudom (2013) attributed this behavior to confinement which is expected to be higher for thicker ice experienced by the wider structure.

From Figure 1, Table 2 summarizes values derived for the parameters C and q in the PA relationship (Eq. 1). Values in parentheses correspond to $q= -0.5$. C and q were derived using a curve fitting application (cftool) in Matlab. The table shows that when indenters of different radii are used, the values of C and q change. The value of q shows no systematic dependence on indenter radius, but C increases with increasing radius, Figure 3. Taking $q= -0.5$, the corresponding value of C scales with radius as C=1.9R (R is in meters) with a goodness of fit of R^2=0.69. For very small indentation depth (i.e., of the order of a few grain diameters), the absolute value of q increases (see test with 200 mm indenter in Table 1), implying a lower limit to the validity of the pressure-area relation (more below).

To summarize, the data from indentation tests on polycrystalline, freshwater ice rapidly loaded by a spherically shaped indenter at -10^{o} C exhibit *two* size effects:

1. *an indentation size effect* in which indentation pressure decreases as the size of the loaded area increases. The relationship $p=CA^q$ is found to hold for indenters submerged almost to

their diameters. However, for loads giving small indentations with respect to the grain diameter, the relationship is inapplicable; and

2. *an indenter radius effect* in which, for a given contact area, indentation pressure increases with increasing radius of the indenter.

3. Explanation of the pressure-area curve in terms of materials behavior

The discussion in this section centers on placing the behavior of ice within the context of materials behavior as a whole.

3.1. Definitions

Within the context of materials behavior, indentation pressure is equivalent to *hardness* –the material resistance to inelastic deformation by indentation. Like indentation pressure, hardness H was defined by Meyer in 1908 and described by Barnes et al. (1971) for ice and by Tabor (2000) for metals as:

$$H = p = \frac{F}{\pi a^2} \qquad \textbf{[2]}$$

where F is the indentation force and a is the chordal radius of indentation, Figure 4. Unlike indentation of ice, an indentation test on a metallic (or ceramic) material usually consists of performing an indent at the surface of the material by the penetration of a rigid indenter at a given indentation load for a given time.

Further, we define a 'representative' stress σ acting on the whole material beneath the indenter, even though stress varies spatially. The representative stress is a function of hardness σ=f(H). Also, we define a 'representative' inelastic strain (Eq. 3a and 3b) within the contact zone, even though strain also varies spatially. We consider two definitions of strain. One is from Tabor (2000):

$$\varepsilon = \phi\left(\frac{a}{R}\right) = m\left(\frac{a}{R}\right)^{\beta} \qquad \textbf{[3a]}$$

where m, β are material constants with positive values and R is the radius of the indenter. The other definition of strain is one that we introduce:

$$\varepsilon = \psi\left(\frac{u}{a}\right) = \frac{u}{s \cdot a}\,, \qquad \textbf{[3b]}$$

where u is the penetration distance and s is a non-dimensional factor, such that the product $s \cdot a$ characterizes the depth at which the inelastic strain is almost zero.

To relate indentation area to strain, we note that for a spherically-shaped indenter the projected area A is a function of u:

$$A = \pi(2Ru - u^2)\,. \qquad \textbf{[4]}$$

Solving Eq. (4) with respect to u and taking into account the fact that the maximum indentation is limited to the indenter radius, we get:

$$u = R - R\sqrt{1 - \frac{A}{\pi R^2}}\,. \qquad \textbf{[5]}$$

Given that $A=\pi a^2$ we can then rewrite strain in terms of area. Then Eq. 3a:

$$\varepsilon = m\left(\frac{\sqrt{A}}{\sqrt{\pi}R}\right)^{\beta} \qquad \textbf{[6a]}$$

and from Eq. 3b:

$$\varepsilon = \sqrt{\pi}\,\frac{1}{s\sqrt{A}}\left(R - R\sqrt{1-\frac{A}{\pi R^2}}\right). \qquad \textbf{[6b]}$$

Since the representative stress is a function of hardness, we can express pressure/hardness-area curves in terms of stress-strain characteristics. For comparison, Figure 5 presents schematic stress (pressure/hardness)-strain (area) curves for ductile metals and brittle ceramics and for ice. Ductile metals exhibit strain hardening (Tabor, 2000), while ceramics (Gong et al., 1999) and ice (Golding et al., 2012) exhibits strain softening once terminal failure sets in. The *q*-values in Figure 5 are justified below.

3.2. Materials-based explanation of size effects

Before accounting for the hardness (pressure)-area relationship in ice, we first describe similar relationships for metals, ceramics and rocks, to show how ice fits a pattern exhibited by other materials.

3.2.1. Ductile solids (e.g., metals)

For ductile metals, Tabor (2000) expressed the constitutive stress-strain relationship as:

$$\sigma = b\varepsilon^{\alpha}, \qquad \textbf{[7]}$$

where $\alpha>0$ represents strain-hardening behavior and ε is described by Eq. 3a. Then from Eq. 2:

$$H = p = \frac{F}{\pi a^2} = c\sigma . \qquad \textbf{[8]}$$

where c is a constant. Equation 8 may be rewritten as:

$$H = p = cb\left(\phi\left(\frac{a}{R}\right)\right)^{\alpha} = cbm^{\alpha}\left(\frac{a}{R}\right)^{\alpha\beta} = cbm^{\alpha}\left(\frac{1}{R}\right)^{\alpha\beta} A^{0.5\alpha\beta}\pi^{-0.5\alpha\beta} = CA^{q}, \qquad \textbf{[9]}$$

where $C = cbm^{\alpha}R^{-\alpha\beta}\pi^{-0.5\alpha\beta} = kR^{-2q}$ and $q = 0.5\alpha\beta$. For ductile metals, α and β, and hence q have positive values (Tabor, 2000), and so for that material, the hardness/pressure *increases* with increasing area of indentation and the coefficient C *decreases* with increasing radius of the indenter. This behavior is a direct result of the strain hardening character of metals and is opposite the behavior exhibited by ice.

The fact that $q>0$ for metals is evident from Meyer's (1908) law. That law states that for an indenter of fixed diameter, the relationship between the load F and the chordal diameter $2a$ of the indent is $F=k_m(2a)^n$, where k_m and n are constants for the metal under examination. Dividing Meyer's expression by the area of indentation $A=\pi a^2$ and expressing a via A, we obtain the following hardness-area relation $H=p=CA^q$, where $C=2^n\cdot\pi^{-0.5n}\cdot k_m$ and $q=0.5n-1$.

Tabor (2000) noted that for ductile metals Meyer's exponent n is generally greater than 2.0 and usually lies between 2.0 and 2.5. Consequently, for metals, q lies between 0.0 and 0.25. Meyer (1908) found experimentally that the index q was almost independent of R but C was proportional to R^{-2q}. Equation 9 derived from stress-strain relationship supports this observation. Tabor (2000) added that, because at very small loads deformation is essentially elastic, there is a lower limit to the validity of Meyer's law, given as a/R=0.1.

3.2.2. Brittle solids (e.g., ceramics and rock)

For ceramics, the relationship between hardness and contact area (or indentation size effect) is opposite that of metals and similar to that of ice. The relationship may be expressed using Auerbach's (1891) law. The law states that the force F required to produce a cone crack is proportional to the radius of the indenter R such that $F=k_aR$, where k_a is the Auerbach constant. Rock, too, obeys Auerbach's law (Lundquist, 1981, Momber, 2004). Following Fischer-Cripps (2007), we can rewrite F in terms of the chordal radius a using Hertzian contact equations for a spherical indenter and a flat surface. Accordingly:

$$F = \left(\frac{4}{3}k_a E^*\right)^{0.5} a^{1.5}, \qquad \textbf{[10]}$$

where E^* is an effective elastic modulus that takes into account Poisson's ratio and the modulus of both the indenter and the specimen. (The expression for E^* can be found in Fischer-Cripps (2007)). We can rewrite Eq. 10 as p=F/A=CA^q, where

$$C = \left(\frac{4}{3}\frac{1}{\pi^{1.5}}k_a E^*\right)^{0.5} \qquad \textbf{[11]}$$

and q= –0.25. Moreover, Gong et al. (1999) pointed out that Meyer's law is applicable to a variety of ceramics and that for those materials Meyer's exponent n= 1.5 to 2. Correspondingly, q= –0.25 to 0.0. A satisfactory explanation of the physical meaning of these relationships (for both ceramics and rock) is still lacking, but may reside in the explanation we propose below for ice.

3.2.3. Polycrystalline ice

Returning to the two size effects observed for ice, we base our interpretation on the strain softening behavior that ice exhibits once terminal failure is reached. The indentation analysis presented in this section assumes that the representative volume of the material has passed through the point of terminal failure such that strain softening takes place. This is a reasonable assumption because characteristics of brittle compressive failure (i.e., radial cracks, saw-tooth load behavior) were evident in all tests considered. Strain softening is evident from compressive stress-strain curves when ice is rapidly loaded (to impart brittle behavior) under triaxial states of stress (e.g., see Golding et al., 2012).

Following Tabor's (2000) analysis for metals, the principal difference for ice is that α<0 (in Eq. 7). This implies that $q<0$, as observed. It could then be said that ice exhibits an 'inverse' indentation size effect, relative to the one seen in metals. Correspondingly, the value of the constant C in the PA relationship is expected to increase with increasing R, as shown in Figure 3.

Qualitatively, therefore, the two size effects exhibited by the indentation of ice can be explained in terms of its strain softening behavior. Quantitatively, we caution against quantifying both C and q from Eq. 9 as we do not have independent measurements of the material constants in that relationship.

The two size effects can also be derived phenomenologically by using the second definition of strain, Eq. 3b. Accordingly, consider two indenters of radii R_l and R_s such that $R_l > R_s$. When the chordal radii of imprints left by indenters are equal $a_l = a_s$ (i.e., the contact area A is the same), the smaller radius indenter creates a deeper crater, i.e., $u_s > u_l$ where u is the depth of imprint. Assuming that both u_s and u_l fulfill the requirements of continuity, we then can establish the ratio of strain created by the smaller radius indenter to that created by the larger radius indenter.

$$\frac{\varepsilon_s}{\varepsilon_l} = \frac{u_s a_l}{u_l a_s} = \frac{u_s}{u_l}, \qquad \textbf{[12]}$$

assuming that $s_l = s_s$.

Substituting Eq. 5 into Eq. 12 we get:

$$\frac{\varepsilon_s}{\varepsilon_l} = \frac{1}{f_1}\frac{(1-\sqrt{1-f_2})}{(1-\sqrt{\frac{f_2}{f_1^2}})}, \text{ where } f_1 = \frac{R_l}{R_s} \text{ and } f_2 = \frac{A}{\pi R_s^{\,2}}. \qquad \textbf{[13]}$$

Moreover, $f_1 \geq 1.0$ and $0 < f_2 \leq 1.0$. The ratio of strains is weakly dependent on the magnitude of f_2 , as can be seen by plotting $\varepsilon_s/\varepsilon_l$ against f_2 for different values of f_1. (For example, for $f_1 = 2.0$, $\varepsilon_s/\varepsilon_l$ approaches a constant value equal to f_1). Hence, the representative strain generated by the smaller radius indenter is higher than that generated by the larger radius indenter.

Now we relate the strains to the stress levels. Figure 6 shows stress vs. time and strain vs. time plots obtained by Golding et al. (2012) from ice loaded triaxially under high degree of confinement. From Figure 6, assuming that strain softening will continue to large strains, one can see that, the representative stress (σ_{11}) is expected to be higher for the larger radius indenter and so does the hardness. This means that for a given contact area *A*, the hardness under the larger radius indenter will be higher than that under the smaller radius indenter. It can also be interpreted that *C* in the equation $p=CA^q$ gets larger with increasing the radius of indenter. This is indenter radius effect we were looking for.

To summarize, we have applied two slightly different definitions of inelastic strain in an attempt to explain two size effects observed during the indentation of polycrystalline ice. First, we borrowed the definition of strain from metallic materials and applied the continuum indentation analysis of Tabor (2000). In the second approach, we used another definition of strain that takes into account the size of the deformation region below the indenter. We utilized the experimentally found stress-strain relationship for the ice loaded tiaxially under high degrees of confinement. In so doing, we were able to account for both the indentation size effect and the indenter radius effect.

4. Discussion

Ice pressure is a function of many variables not just the contact area. But, in Sanderson's PA relation, the other variables are hidden in the proportionality constants *C* and *q*. This paper has re-examined full and laboratory scale data on freshwater ice indentation with spherically-shaped indenter tips and has addressed two questions. Firstly, given the PA relation (Eq. 1), do *C* and *q* relate to the material properties of ice and to the system parameters of the indenter? The answer is yes, as taking into account strain-softening behavior of ice, the parameters *C* and *q* can be expressed in terms of material parameters (strain softening exponent, etc.); see Eq. 9. Secondly, for a given spherical indenter tip, do *C* and *q* vary with indenter tip radius? The analysis in this paper has shown that that the coefficient *C* increases with increasing size of the indenter, but the exponent q shows no systematic dependence on radius.

So, what do we have now on Sanderson's pressure-area relationship $p=CA^q$ that the earlier explanations (i.e., Palmer and Sanderson (1991), Palmer et al. (2009), Sanderson (1988) and Schulson and Duval (2009)) did not offer? In short, we have shown that the indentation of ice exhibits two effects of size, and we have developed greater physical insight into the coefficient C and the exponent q. Also, we have an appreciation that ice, when indented within the regime of brittle behavior, reflects behavior exhibited by other materials.

On size effects, in examining only data that have been obtained under more or less one set of conditions – indenter shape (spherical), temperature, rapid loading, confined freshwater ice – we have shown that indentation pressure depends on both indentation size and indenter radius, and that both effects can be explained in terms of the stain softening behavior of ice when rapidly deformed beyond the point of terminal failure. We expect that indenters of other shapes may lead to similar effects.

On the parameters in Sanderson's relationship, earlier explanations found that $q<0$ for global pressure and, depending on which model one favored, led to specific, but different values: –0.5, –0.27, –0.25, –1.0. The present, constitutive based model also finds that $q<0$, but does not specify one value. Instead, the new model expresses q in terms of the product of the strain softening exponent α (Eq. 7) and the exponent β that relates inelastic strain to the ratio of the radii of the indentation and the indenter (Eq. 3a), $q= -0.5\alpha\beta$. At this juncture, there are no data available on the value of the either exponent, only the qualitative results (from stress-strain curves in Figure 6) that $\alpha<0$ beyond the point of terminal failure and that $\beta>0$. It is premature, therefore, to go further than we have. Our sense, however, is that the actual value of both exponents may be a function of the conditions of deformation (temperature, indentation velocity, grain size of the ice, etc.) and, thus, that the value of q depends somewhat on the conditions of indentation. From a practical perspective, however, the value $q = -0.5$ seems to describe field data quite well.

In terms of the coefficient C, earlier models were not informative. The present model, in comparison, expresses C algebraically in terms of a number of materials parameters (Eq. 9) and indenter radius. Again, since the values of material parameters are not available, it is difficult to specify C numerically. Yet, with respect to the objective of this study, the new model shows that C increases with the radius of the indenter, owing to the strain softening character of ice ($\alpha<0$).

Finally, the constitutive-based explanation has placed ice within the context of non-linear inelastic behavior of materials as a whole.

5. Summary and conclusions

This paper has been concerned with the situation where a hard, spherically shaped indenter of radius between 5 and 2300 mm is pressed rapidly into the flat surface of polycrystalline, freshwater ice at approximately –10° C. This paper has addressed two questions regarding the pressure-area relationship for the indentation of ice: do the proportionality constants between the ice pressure and contact area relate to the material properties of ice and to the system parameters of the indenter, and do these proportionality constants vary with indenter radius.

Analysis of field and laboratory data has shown that:

- There are two effects of size on indentation pressure: an *indentation size effect* and an *indenter radius effect*. The indentation size effect means that the contact pressure p (hardness) decreases as the magnitude of the loaded area A increases. Accordingly, for conditions of brittle behavior, the relationship $p=CA^q$ is found to hold for spherical indenters submerged almost to their diameters, where $q<0$.

However, for loads giving small indentations with respect to the grain size of the ice, the relationship does not apply. The indenter radius effect means that, for a given contact area, indentation pressure (hardness) increases with increasing radius of the indenter; i.e., that the coefficient C increases with increasing size of the indenter, but q is weakly dependent on radius.

- The pressure-area relationship reflects semi-quantitatively the stress-strain constitutive relationship for ice as a material, particularly the strain-softening of ice when deformed beyond terminal failure within the regime of brittle behavior. In this regard, the indentation of ice is reminiscent of the indentation of metals, ceramics and rock.
- A continuum indentation analysis, taking into account the strain softening character of the ice, can account for the two size effects.

In the context of structure-ice interactions, the information presented in this paper can be helpful in establishing or interpreting the coefficients in the PA relationship for the scenarios of indentation into an ice wall. The link between a constitutive stress-strain relationship for ice and the resulting pressure-area dependency can be used in future mathematical models of ice crushing.

Acknowledgments

The authors acknowledge support from Research Council of Norway through the Centre for Research-based Innovation SAMCoT and support from all SAMCoT partners, from the US-Norway Fulbright Foundation and from the Norwegian University of Science and Technology (Trondheim). The work is also a part of investigations conducted within the AMOS (Centre for Autonomous Marine Operations and Systems) Centre of Excellence.

References

Auerbach, F., 1891. Absolute Härtemessung. Annalen der Physik und Chemie 43, 61–100.

API Recommended Practice 2N, 1995. Planning, designing and constructing structures and pipelines for Arctic conditions. American Petroleum Institute: 2nd edition.

Barnes, P., Tabor, D. and Walker, J.C.F., 1971. The friction and creep of polycrystalline ice. Proceedings of the Royal Society of London A: Mathematical, Physical and Engineering Sciences 324(1557), 127–155.

Blanchet, D. and DeFranco, S., 2001. On the understanding of the local ice pressure area curve. In the Proceedings of IUTAM Symposium on Scaling Laws in Ice Mechanics and Ice Dynamics, 13–30.

CAN/CSA-S471-04, 2004 General requirements, design criteria, the environment, and loads. National Standard of Canada, Canadian Standards Association.

DNV Rules for Classification of Ships, 2013. Ships for Navigation in Ice. Det Norske Veritas AS.

Fischer-Cripps, A.C., 2007. Introduction to contact mechanics. Springer: 2nd edition, 226p.

Golding, N., Schulson, E.M. and Renshaw, C.E., 2012. Shear localization in ice: Mechanical response and microstructural evolution of P-faulting. Acta Materialia 60, 3616–3631.

Gong, J., Wu, J. and Guan, Z., 1999. Analysis of the indentation size effect on the apparent hardness for ceramics. Material Letters 38, 197–201.

IACS, 2011. Requirements concerning Polar Class, International Association of Classification Societies Ltd.

ISO 19906, 2010. Petroleum and natural gas industries – Arctic offshore structures. International standard: 1st edition.

Kim, E., Golding, N., Schulson, E.M., Løset, S. and Renshaw, C.E., 2012. Mechanisms governing failure of ice beneath a spherically-shaped indenter. Cold Regions Science and Technology 78, 46–63.

Lundqvist, R.G., 1980. Hemispherical indentation and the design of “Button Bits” for Percussive Drilling. In Proceedings of the 22nd U.S. Symposium on Rock Mechanics, 219–222.

Masterson, D.M. and Frederking, R.M.W., 1993. Local contact pressures in ship/ice and structure/ice interactions. Cold Regions Science and Technology 21, 169–185.

Masterson, D.M., Frederking, R.M.W., Wright, B., Kärnä, T. and Maddock, W.P., 2007. A revised ice pressure–area curve. In Proceedings of the 19th International Conference on Port and Ocean Engineering under Arctic Conditions 1, 305–314.

Masterson, D.M., Nevel, D.E., Johnson, R.C., Kenny, J.J. and Spencer, P.A., 1992. The medium scale iceberg impact test program. In Proceedings of the 11th International Symposium on Ice 2, 930-966.

Meyer, E., 1908. Untersuchungen über Härteprüfung und Härte. Zeitschrift des Vereins Deutscher Ingenieure 52(17), 645–654.

Momber, A.W., 2004. Deformation and fracture of rocks loaded with spherical indenters. International Journal of Fracture 125, 263–279.

Palmer, A.C. and Sanderson, T.J.O., 1991. Fractal crushing of ice and brittle solids. Proceedings of Mathematical and Physical Sciences 433(1889), 469–477.

Palmer, A.C., Dempsey, J.P. and Masterson, D.M., 2009. A revised ice pressure-area curve and a fracture mechanics explanation. Cold Regions Science and Technology 56, 73–76.

Sanderson, T.J.O., 1988. Ice mechanics. Risks to offshore structures. Graham and Trotman, London, UK.

Schulson, E.M. and Duval, P., 2009. Creep and fracture of ice. Cambridge University Press. 401p.

Sodhi, D.S., 2001. Crushing failure during ice–structure interaction. Engineering Fracture Mechanics 68(17–18), 1889–1921.

Tabor, D., 2000. The hardness of metals. Oxford University Press, 175p.

Timco, G.W. and Frederking, R.M.W., 1993. Laboratory impact tests on freshwater ice. Cold Regions Science and Technology 22, 77–97.

Timco, G.W. and Sudom, D., 2013. Revisiting the Sanderson pressure-area curve: Defining parameters that influence ice pressure. Cold Regions Science and Technology 95, 53–66.

Appendix A

Small-scale laboratory ice indentation tests (Kim et al., 2012)

Load-time and displacement-time curves were used to access ice pressure. For each test, the local load-peaks were used to calculate pressures between the surface of the indenter and the indentation. Projected contact area at a given peak load was determined using the corresponding displacement of the indenter. The pressure was calculated as the ratio of the load to the projected area of indentation at the corresponding time step and corresponded to global ice pressure.

Medium-scale indentation tests (Masterson et al., 1992)

Masterson et al. (1992) and Masterson and Frederking (1993) used local peaks of the load-time histories to construct pressure-area plots. The pressure on the projected area of the indenter was calculated as the measured load from the load cells divided by the contact area at the time of peak load. The surface contact area, calculated from indenter penetration as a function of time, was used in the pressure calculations because for the maximum penetration, the difference between the projected and surface area was 5 percent or less. To access global pressures for the tests, we digitized using Java program "Plot Digitizer" the data available in Figure 14 of Masterson et al. (1992) and in Figure 6 of Masterson and Frederking (1993) for spherically shaped indenters.

Laboratory impact tests (Timco and Frederking, 1993)

Timco and Frederking (1993) calculated the average pressure as the ratio of the impact force (F) to the area (A) at the corresponding time step using force-time and displacement-time curves. The impact force, in turn, was calculated from the measured acceleration (a_z) and known mass of the indenter (M) as $F=Ma_z$. The area of contact throughout the impact (A) was calculated from the geometries of the ice and the indenter by determining the penetration depth as a function of time from the acceleration record. To access pressures for the tests, we digitized (again using Java program "Plot Digitizer") the data available in Figure 17 of Timco and Frederking (1993) for a spherically shaped indenter (Test J30-003). This gave us average global pressure versus projected contact area during the impact event.

Tables

Table 1. Summary of various pressure-area relationships in offshore codes and in ships rules; pressure is in units of MPa; subscripts G and L indicate global and local pressure, respectively. The definition of global/local pressure is adopted from Timco and Sudom (2013).

Codes and rules	PA-relation	Contact area	Comments
Canadian Standard Association CSA S471-04, Clause E.6.2.3	p_G=26.9	A≤0.1 m^2	The constant coefficients have been multiplied by factors appropriate for the sea ice
	p_G=8.5$A^{-0.5}$	0.1<A≤30 m^2	

	$p_G=2.7A^{-0.165}$	$A\geq 30$ m^2	regime with annual freezing degree days of 3000 to 4000 °C-days.
ISO (International Standard Organization) 19906, Clause A.8.2.4.3.3	$p_G \approx 2.8A^{-0.15}$ $A = w \cdot h$	$2.0\leq A<200$ m^2	In ISO, the global pressure is used in combination with ice thickness (h) and structural width (w). This pressure-area relation is an approximation for scenarios where first-year or multi-year ice of thickness more than 1.0 m acts against a vertical structure in Arctic areas.
ISO 19906, Clause A.8.2.4.3.5 and Canadian Standard Association CSA S471-04, Clause E.6.2.3 (Random action)	$p_G=C_pA^{D_p}$, where C_p=3.0±1.5, D_p=–0.4±0.2	$A<50$ m^2	Determined using data collected during ship rams in multi-year ice, i.e., from the Kigoriak, Polar Sea, MV Arctic, Manhattan, and Oden icebreaker trials.
ISO 19906, Clause A.8.2.5.3	$p_L=7.40A^{-0.70}$ $p_L=1.48$	$A\leq 10$ m^2 $A>10$ m^2	Determined using data collected by Masterson et al. (2007). These include pressure from interactions with the Molikpaq structure, with Hobson's Choice ice island and also from indenter and flat-jack field tests.
API RP 2N (American Petroleum Institute Recommended Practice), Clause 5.4.7a	$p^a=8.1A^{-0.5}$ $p^a=1.5$	$0.1\leq A\leq 29$ m^2 $A>29$ m^2	Corresponds to the average value +2STD for combined data for on Figure 11 in Masterson and Frederking (1993). These are taken from indenter and from flat-jack field tests, from ship ramming trials and from ice interactions with the Molikpaq structure and with Hobson's Choice ice island.
IACS UR I2 (International Association of Classification Societies Unified Requirements), Background notes to design ice load	$p_G=P_oA^{-0.1}$, where P_o depends on the Polar Class of the vessel and varies between 1.25 6.0.	Calculated based on penetration depth, geometry of the ice edge and of the vessel	For derivation of the oblique collision force on the bow.
DNV (Det Norske Veritas) Rules for Classification of Ships, Part 5, Ch.1, Sec. 4, Clause D 400	$p_L=CA^{-0.50}$ $p_L=CA^{-0.15}$, where C is the correction factor depending on Ice Class and ice reinforced area in question. It varies between 2.4 and 5.8 in the bow and stem area.	$A\leq 1.0$ m^2 $A>1.0$ m^2	The design pressure shall be applied over a corresponding contact area reflecting the type of load in question.

[a] Derivation of pressure is based on the assumption that only one PA curve applies to all design conditions (Blanchet and DeFranco, 2001).

Table 2. Summary of curve fitting parameters.

Indenter	Maximum	C	q	Goodness

radius (mm)	penetration depth (mm)	($MPa \cdot m^{-2q}$)	(-)	of fit R^2
5[a]	5	0.053 (0.22)	–0.64 (–0.5)	0.99 (0.97)
12.7[a]	12.7	0.11 (0.30)	–0.63 (–0.5)	0.98 (0.99)
100	uncertain	0.60 (0.79)	–0.55 (–0.5)	0.68 (0.68)
200	20	$5.6 \cdot 10^{-5}$ (0.24)	–2.3 (–0.5)	0.91 (0.24)
400	40	0.46 (0.92)	–0.74 (–0.5)	0.94 (0.99)
900	90	1.04 (2.1)	–0.92 (–0.5)	0.63 (0.64)
1280	128	4.4 (4.3)	–0.50 (–0.5)	0.90 (0.91)
2300	230	3.3 (3.3)	–0.44 (–0.5)	0.79 (0.99)

[a] tests with constant indentation speed

Table A1. Summary of test parameters for the considered data sets.

Data source	*Kim et al. (2012)*	*Masterson et al. (1992)*	*Timco and Frederking (1993), Test J30-003*
Test type	indentation at a constant speed of 5.08 mm/s	indentation with a speed varying from 100 mm/s at the ice surface to zero after traveling a distance in the ice	drop test with an impact speed of 3700 mm/s
Indenter	hemispherical with R=5.0 mm and 12.7 mm	spherically shaped with R=200 mm, 400 mm, 900 mm, 1280 mm and 2300 mm	spherically shaped with R=100 mm
Ice type	freshwater granular ice (grain size 1 to 2.4 mm)	iceberg ice (effective grain size 10 mm)	freshwater columnar S2 ice (column diameter 1–6 mm) indented along the columns
Temperature	–10°C	–10°C	–12°C
Maximum penetration	0.08R–R	0.1R	0.09R
Time to maximum displacement	0.2–2.5 s	0.3–3.6 s	≈ 0.006 s
Sampling frequency	2 kHz	10 kHz	50 kHz

Figure captions

Figure 1. Summary of pressure-area data from indentation and impact tests on freshwater ice with spherical indenters of different radii.

Figure 2. Compilation plots of all measurements on field structures where the ice failed in a crushing mode; source: Timco and Sudom (2013), Figures 20 and 21.

Figure 3. Indentation of freshwater, polycrystalline ice. Plot of C against R. Data taken from Table 1; C values are for q of –0.5.

Figure 4. Illustration of the indentation problem (a–chordal radius of indentation, $u(t)$ –penetration depth, $F(t)$–indentation force, R–radius of the indenter).

Figure 5. Schematic representation of stress vs. strain relationship (or hardness vs. area curve) for ductile and brittle solids; logarithmic scales.

Figure 6. Stress vs. time and strain vs. time from freshwater ice loaded at temperature of –10°C and $\dot{\varepsilon}_{11} = 3\times10^{-2}$ 1/s. Note that for an indentation test the first principal stress (σ_{11}) is expected to be smaller due to shear (data from Golding et al., 2012).

Figures

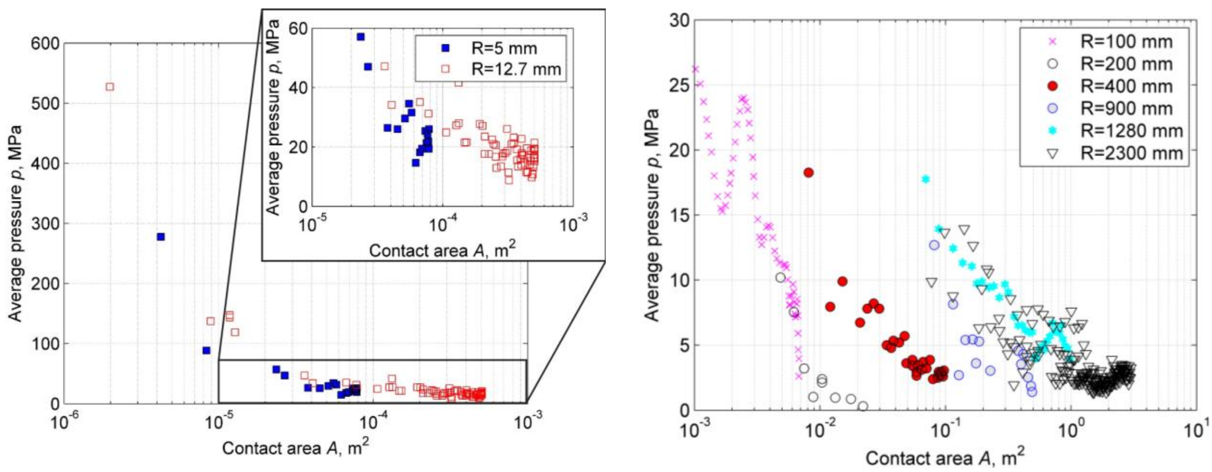

(a) Constant indentation speed (unlimited energy in the interaction)

(b) Variable indentation speed (limited energy)

Figure 1.

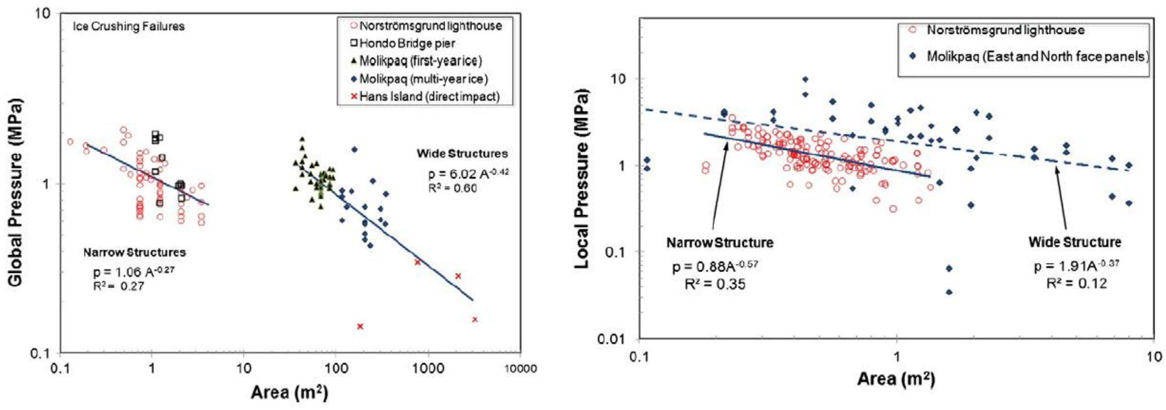

(a) Global pressure vs. area

(b) Local pressure vs. area

Figure 2.

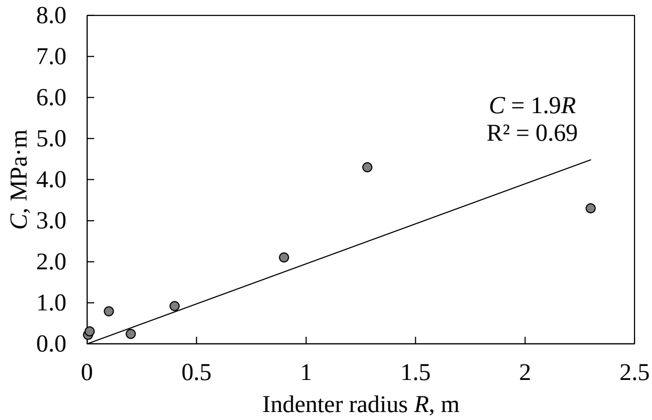

Figure 3.

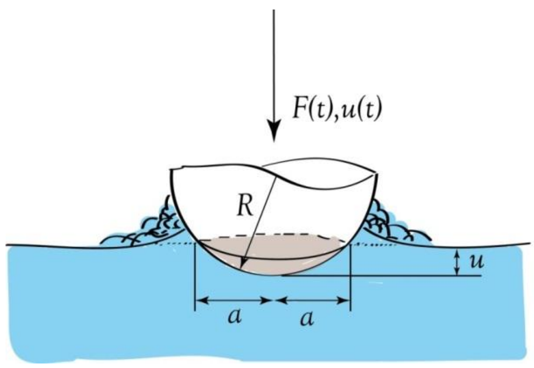

Figure 4.

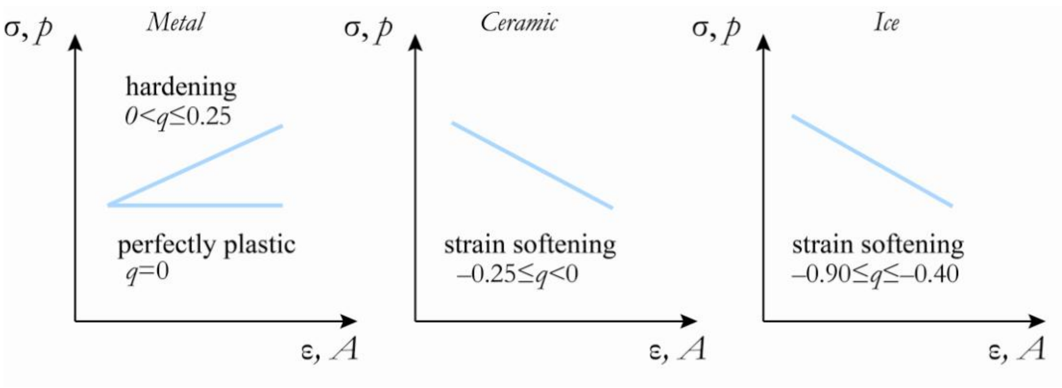

Figure 5.

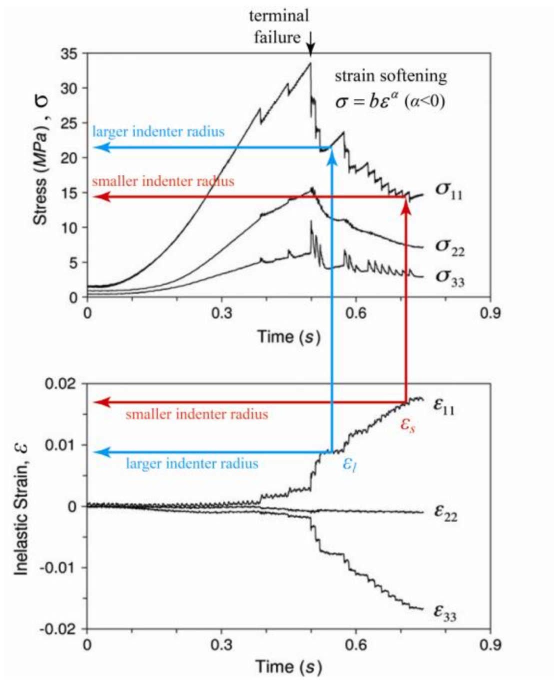

Figure 6.